Infrared spectroscopic study of $CaFe_{0.7}Co_{0.3}O_3$

C. X. Zhang,[1] H. L. Xia,[1] Y. M. Dai,[2] Z. Y. Qiu,[1] Q. T. Sui,[1] Y. W. Long,[1,3] and X. G. Qiu[1,3]

[1]*Beijing National Laboratory for Condensed Matter Physics, Institute of Physics, Chinese Academy of Sciences, P.O. Box 603, Beijing 100190, China*

[2]*Center for Superconducting Physics and Materials, National Laboratory of Solid State Microstructures and Department of Physics, National Collaborative Innovation Center of Advanced Microstructures, Nanjing University, Nanjing 210093, China*

[3]*Collaborative Innovation Center of Quantum Matter, Beijing 100190, People's Republic of China*

(Received 12 May 2017; published 24 August 2017)

Temperature-dependent infrared spectroscopy has been investigated for $CaFe_{0.7}Co_{0.3}O_3$ which undergoes a ferromagnetic transition at $T_C \approx 177$ K. It is observed that the spectral weight is transferred from ~4800–14 000 cm^{-1} to ~0–4800 cm^{-1} as the temperature is lowered around T_C. Such a large-range spectral weight transfer is attributed to the Hund's interaction. The phonons in $CaFe_{0.7}Co_{0.3}O_3$ show minor asymmetric line shapes, implying relatively weak electron-phonon coupling compared with the parent compound $CaFeO_3$. The optical conductivity also reveals a broad peak structure in the range of ~700–1500 cm^{-1}. Fit by the model of single-polaron absorption, the broad peak is interpreted by the excitation of polarons. From the fitting parameters of the polaron peak, we estimate the electron-phonon coupling constant $\alpha \sim 0.4$–0.5, implying that $CaFe_{0.7}Co_{0.3}O_3$ falls into the weak-coupling regime.

DOI: 10.1103/PhysRevB.96.075154

I. INTRODUCTION

Strongly correlated electronic systems have been attracting a tremendous amount of research activity because they often exhibit peculiar phenomena such as high-temperature superconductivity, colossal magnetoresistivity, and charge-disproportionation (CD) transition [1]. Extensive studies on these systems have revealed important cooperations among charge, spin, and lattice degrees of freedom. Take doped perovskite manganites for example, various charge- and spin-ordered phases emerge due to the collective effects of electron correlation, double-exchange interaction, and electron-lattice coupling [2].

Theoretical work by Millis *et al.* [3] based on double-exchange interaction and electron-lattice coupling implies that the phase diagram can be mainly divided into three regimes, according to the electron-phonon coupling strength. In the weak-coupling regime, a metallic paramagnetic (PM) phase is transformed into a metallic ferromagnetic (FM) phase upon cooling. In the intermediate/strong-coupling regime, an insulating PM phase is transformed into a metallic/insulating FM phase, respectively. Therefore, the strength of the electron-phonon coupling is pivotal to determine the position of the system in the phase diagram. However, due to the difficulties in extracting the electron-phonon coupling constant [4–6], the doping effects on the coupling in manganites have not been studied thoroughly.

The interaction of lattice, charge, and spin degrees of freedom also exists in the perovskite $CaFe_{1-x}Co_xO_3$ (CFCO). The parent compound ($x = 0$) $CaFeO_3$ exhibits a CD transition alongside a breathing-type lattice distortion at 290 K, which transforms the compound from an orthorhombic metal to a monoclinic insulator [7]. At a relatively low temperature ~118 K, it undergoes a helical antiferromagnetic (AFM) transition [7]. When x falls in the interval $0.2 < x < 0.5$, the compound undergoes a metallic PM-FM transition at ~150–200 K [8]. Compared to $La_{1-x}Ca_xMnO_3$ (LCMO) with $0.2 < x < 0.4$, which has a phase transition from an insulating PM state to a metallic FM state, the CFCO system provides a different platform to study the weak-coupling regime of the phase diagram proposed by Millis *et al.* [3]. Furthermore, comparative studies among the samples in the CFCO system are helpful to investigate the CD mechanism in the parent compound $CaFeO_3$.

Infrared (IR) spectroscopy is a powerful tool to study lattice, charge, and spin dynamics, as well as interactions among them [9–11]. Electron-phonon interactions often manifest themselves as asymmetric phonon line shapes and broad polaronic peaks [12–15]. The asymmetric phonon line shapes can often be described by the Fano profile, and the degree of asymmetry is specified by the Fano factor q, which is related to the strength of electron-phonon interaction. The optical response of LCMO with $x \sim 0.3$ has been extensively investigated. Hartinger *et al.* [16] reported Fano-like phonon line shapes, and Kim *et al.* [4] observed polaronic peaks at about 1000 cm^{-1} in LCMO. Both of them [4,16] claimed that strong electron-phonon coupling existed in LCMO. Moreover, it has been observed that as the temperature is lowered around T_C, the spectral weight is transferred from the high- to the low-energy region on a large energy scale, which is attributed to the Hund's interaction [4]. In $CaFeO_3$, the Fano line shapes and wide-range spectral weight transfer are also observed [17,18].

In the present work, we investigate the compound $CaFe_{0.7}Co_{0.3}O_3$ by IR spectroscopy. Having the same crystal structure as $CaFeO_3$, $CaFe_{0.7}Co_{0.3}O_3$ does not exhibit a CD transition but undergoes a PM-FM transition [19] around 177 K. We found that with decreasing temperature, the spectral weight is transferred over a large energy region, and a broad polaronlike peak appears in the mid-IR region. Assuming its polaronic nature, we fit the data by the model of Gurevich *et al.* [20] and find that the temperature dependence of the peak is consistent with the polaronic behaviors found in $La_{0.7}Sr_{0.3}MnO_3$ (LSMO) [6]. Furthermore, from the fitting parameters of the polaronic peak, the electron-phonon coupling constant α is estimated to be ~0.4–0.5, which is much smaller

than the one found in LCMO [4]. Besides, the phonon peaks in this CFCO compound only show minor asymmetric line shapes, implying relatively weak electron-phonon coupling compared with the parent compound $CaFeO_3$. It also implies that the electron-lattice interactions play important roles in the CD transition in the parent compound.

II. EXPERIMENT

Single crystals of $CaFe_{0.7}Co_{0.3}O_3$ were grown by a two-step synthesis method combining a floating-zone technique and high-oxygen-pressure treatment [21,22]. The temperature-dependent resistivity and magnetic susceptibility reported by Xia *et al.* [19] shows $T_C \sim 177$ K.

The reflectivity $R(\omega)$ was measured at a near-normal angle of incidence on a Fourier transform infrared spectrometer (Bruker 80v). An *in situ* gold overfilling technique [23] was used to obtain the absolute reflectivity of the samples. Data from 70 to 15 000 cm^{-1} were collected at different temperatures ranging from 15 to 300 K. $R(\omega)$ in the visible and UV range was measured up to 40 000 cm^{-1} at room temperature with an AvaSpec-2048 × 14 optical fiber spectrometer.

III. RESULTS AND DISCUSSIONS

A. Reflectivity and optical conductivity

Figure 1(a) shows the temperature dependence of $R(\omega)$ of $CaFe_{0.7}Co_{0.3}O_3$ below 25 000 cm^{-1}. Unlike the parent compound [17,18], $R(\omega)$ of $CaFe_{0.7}Co_{0.3}O_3$ below 6000 cm^{-1} increases with lowering temperature, while the spectra around 10 000 cm^{-1} decrease. Above 14 000 cm^{-1}, the spectra are almost temperature independent, and the spectra at different temperatures cross at about 6600 cm^{-1}. In the low-energy region, $R(\omega)$ increases toward unity with decreasing photon energy, indicating its metallic nature in the whole temperature range. As a comparison, the temperature dependence of $R(\omega)$ of the parent compound $CaFeO_3$ is shown in Fig. 1(b). It might also be interesting to compare $R(\omega)$ shown in Fig. 1(a) with the reflectivity spectra of $SrFeO_3$ [17], whose shapes and temperature dependence are similar to the present case. However, we notice that each spectrum in Fig. 1(a) shows a kink structure, marked by the arrow at about 780 cm^{-1}, which is not clear in the spectra of $SrFeO_3$ [17].

In order to obtain the optical conductivity, Kramers-Kronig analysis of $R(\omega)$ in Fig. 1(a) is performed. At low frequency, the Hagen-Rubens extrapolation ($R = 1 - A\sqrt{\omega}$) is employed. Above 40 000 cm^{-1}, a constant reflectivity up to 12.5 eV is utilized, followed by a free-electron (ω^{-4}) response. Figure 2(a) shows the real part of the optical conductivity $\sigma_1(\omega)$ at different temperatures. As the temperature is lowered, $\sigma_1(\omega)$ below 4800 cm^{-1} increases upon the whole, and the Drude peak becomes more evident. On the other hand, the spectra around 10 000 cm^{-1} decrease with lowering temperature. Sharp peaks below 700 cm^{-1} represent IR-active phonons. As a comparison, $\sigma_1(\omega)$ data of $CaFeO_3$ [18] at several different temperatures are shown in Fig. 2(b). In addition, from Fig. 2(a), we find a broad peak starting from ~750 cm^{-1} (marked by an arrow), corresponding to the kink structure of $R(\omega)$ in Fig. 1(a).

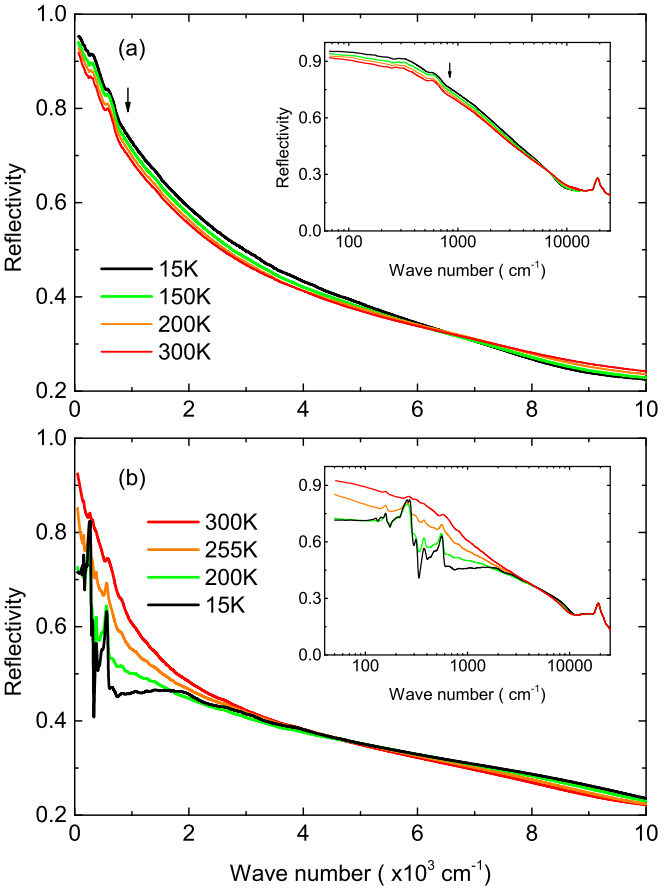

FIG. 1. (a) Reflectivity of $CaFe_{0.7}Co_{0.3}O_3$ at several representative temperatures. (b) Reflectivity of $CaFeO_3$ at several representative temperatures. The insets show the spectra up to 25 000 cm^{-1}. The arrows in (a) denote the kink structure.

B. Spectral weight analysis

From Fig. 2(a), one observes that the spectral weight [the area under the $\sigma_1(\omega)$ curve], defined as $W_a^b = \int_a^b \sigma_1(\omega)d\omega$, transfers from high to low energy with decreasing temperature. To quantify this change, we calculated W in three different energy intervals: 0–700 cm^{-1}, 0–4800 cm^{-1}, and 4800–14 000 cm^{-1}. The temperature dependence of the normalized spectral weight $W(T)/W(300\,\mathrm{K})$ is displayed in Fig. 3, reflecting the spectral weight transfer from the 4800–14 000 cm^{-1} to 0–4800 cm^{-1} region upon cooling, as shown in Fig. 2(a). Consistent with the temperature dependence of magnetic susceptibility measured in the field-cooled mode with $H = 0.1$ T, which is shown in the inset of Fig. 3, the spectral weight transfer accelerates around the Curie temperature $T_C \sim 177$ K, implying a prominent change of spectral weight associated with the PM-FM phase transition. Therefore, it is reasonable to speculate that the FM transition is the origin of the above-mentioned spectral weight transfer. Similar behavior has been found in $Sr_{1-x}Ce_xMnO_3$ where the AFM phase transition induces a spectral weight transfer from low to high energy. Nucara *et al.* [24] explained it in the framework of Hund's coupling, crystal field, and Jahn-Teller splitting. In the present work, we try to explain the opposite

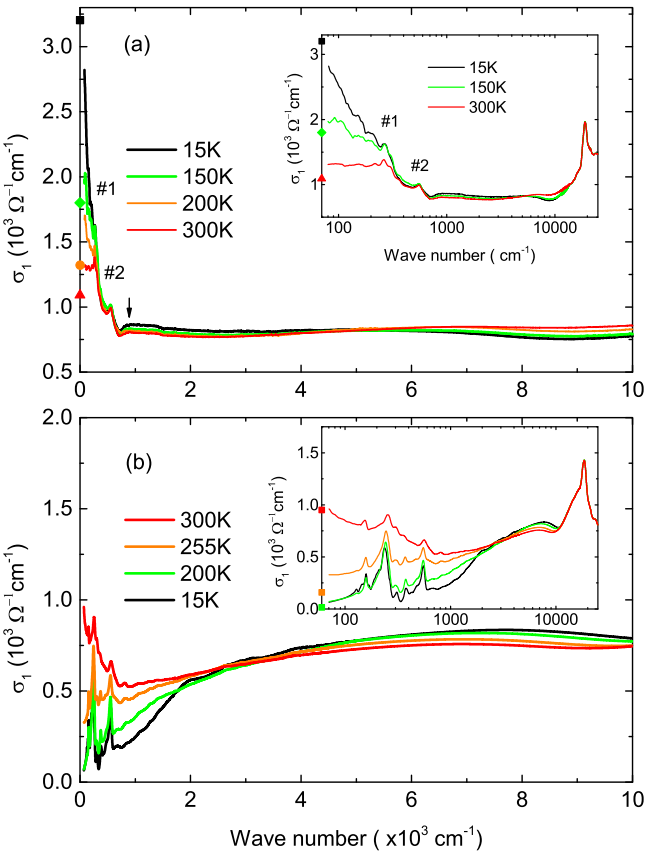

FIG. 2. Optical conductivity for (a) $CaFe_{0.7}Co_{0.3}O_3$ and (b) $CaFeO_3$, respectively. The insets show the spectra up to 25 000 cm^{-1}. The symbols on the vertical axis are dc values of the conductivity obtained from the transport measurement. The arrow in (a) denotes the polaronlike peak related to the kink structure in Fig. 1(a).

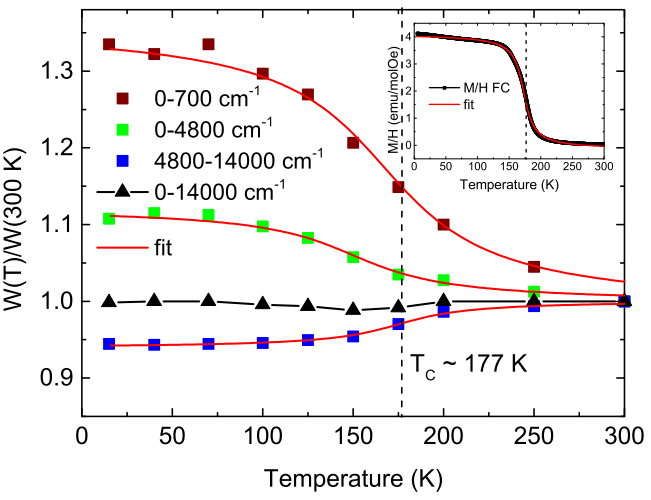

FIG. 3. Temperature dependence of the normalized spectral weight $W(T)/W(300\,\mathrm{K})$ in different energy regions. The dashed line indicates the FM phase transition. The inset is the temperature dependence of the magnetic susceptibility measured in the field-cooled mode with $H = 0.1$ T. The red curves are fittings by the inverse tangent function.

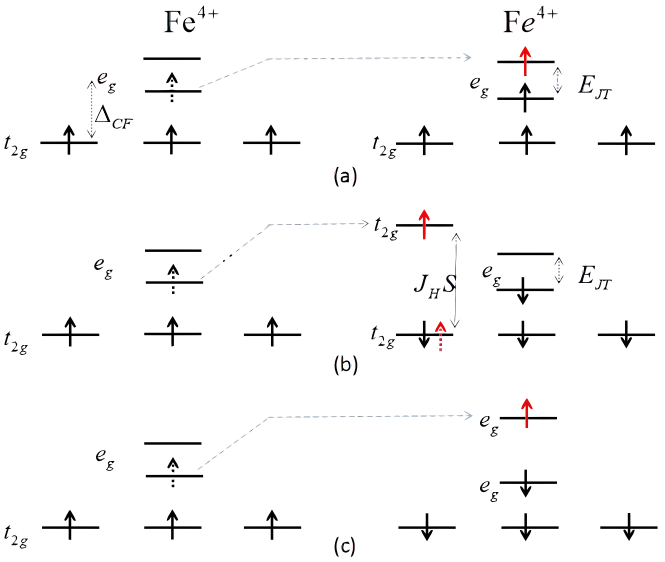

FIG. 4. Schematic energy diagrams describing the hopping of an electron between Fe ions. (a) The type-1 excitations with parallel spins. (b),(c) The type-2 excitations with antiparallel spins. The dashed arrow lines from left to right denote the hopping processes. The black dashed arrows in the left side are the initial states of the hopping electrons, while the red arrows in the right side are the final states of the hopping electrons.

spectral weight transfer in FM $CaFe_{0.7}Co_{0.3}O_3$ similar to the work of Nucara *et al.*

In $CaFe_{0.7}Co_{0.3}O_3$, Fe^{4+} ions have the electronic configuration as $t_{2g}^3 e_g^1$ with Jahn-Teller splitting E_{JT} [19,25]. The energy difference between t_{2g} and e_g is the crystal-field splitting Δ_{CF}. In the high-temperature PM phase, the spins are randomly oriented, but in each ion (Fe^{4+} and Co^{4+}), the spins are polarized due to the Hund's coupling. Similar to the work of Nucara *et al.* [24], we introduce two types of excitations. Type-1 excitation is an e_g electron of Fe/Co ions hopping to a neighboring Fe/Co ion with the same spin, while type-2 excitation is the hopping between ions with different spin directions. Taking the hopping between Fe ions for example, the energy cost for the type-1 excitation is $E_1 = E_{JT} - J_H/4$, shown in Fig. 4(a). As for type-2 excitation, because of the antiparallel spin configuration, an additional energy $J_H S$ should be paid due to the Hund's interaction. J_H is the Hund's coupling and S is the total spin of the Fe^{4+} ion. If the lowest antiparallel state for the hopping electron is t_{2g}, then such type-2 excitation energy is $E_2 = U - U' - \Delta_{CF} + 7J_H/4$, as shown in Fig. 4(b). U and U' are intraorbital and interorbital Coulomb energies, respectively. However, if the lowest antiparallel state is e_g, then the excitation energy is simply $E_2' = E_{JT} + 7J_H/4$, as shown in Fig. 4(c). As the temperature is lowered around T_C, the spins of Fe^{4+} and Co^{4+} ions tend to point in the same direction. Therefore, the type-1 excitation is enhanced while the type-2 excitation is suppressed. Because $E_1 < E_2, E_2'$, the spectral weight is transferred from high to low energy as the temperature is lowered around the FM transition. To get the estimation for the values of E_1, E_2, and E_2', it might be helpful to refer to the band structure [26], from which we obtain

TABLE I. Parameters for the fittings of the temperature dependence of magnetic susceptibility, spectral weights, strength parameters Ω_1 and Ω_3 of Lorentz oscillators, plasma frequency Ω_p, and polaron intensity η by Eq. (1).

	M/H	W_0^{700}	W_0^{4800}	W_{4800}^{14000}	Ω_1	Ω_3	Ω_p	η
k/c	0.7	0.1	0.04	0.02	0.03	0.04	0.02	0.13
t_0 (K)	173	167	150	175	175	175	175	175
Γ (K)	12	45	40	30	48	43	12	22

that $\Delta_{CF} \sim 2$ eV, $E_{JT} \sim 0.5$ eV, $J_H \sim 1$ eV. Therefore [27], $U - U' = 2J_H \sim 2$ eV, $E_1 \approx 0.25$ eV ~ 2000 cm^{-1}, $E_2 \approx 2.25$ eV $\sim 18\,000$ cm^{-1}, and $E_2' \approx 1.75$ eV $\sim 14\,000$ cm^{-1}.

In order to study the relationship between the spectral weight transfer and the FM transition, we quantitatively compare the temperature dependence of the spectral weight and magnetic susceptibility through a phenomenological fitting. The magnetic susceptibility curve shows a broad temperature range of transition and the curve is nearly symmetric with respect to $T_C \sim 177$ K. The curve can be fit well by the inverse tangent function,

$$f(T) = c - k \cdot \mathrm{atan}\left(\frac{T - t_0}{\Gamma}\right), \tag{1}$$

with $t_0 = 173$ K and $\Gamma = 12$ K. Then we perform similar fittings for the temperature dependence of the normalized spectral weight in Fig. 3, which can be fit rather well by Eq. (1) with parameters shown in Table I. We find that the t_0's are in the range of ~150–175 K, while the Γ's are much larger than the one for the magnetic susceptibility. It implies that the spectral weight transfer occurs in a much wider temperature range. One of the possibilities is that the magnetic domains form much above $T_C \sim 177$ K, which leads to the spectral weight transfer but do not show up in the magnetic susceptibility because of their random orientations. However, because the magnetic susceptibility is measured under the magnetic field with $H = 0.1$ T, the effects of the preformed domains should be observed from the susceptibility. Another possibility is that dynamic short-range FM orders fluctuate in a wider temperature region. By dynamic FM orders, we mean that the directions of some spins of Fe/Co ions lock to each other, but fluctuate together because of the thermal effects for example. The formation of such dynamic order may lead to a change in the spectral weight, but does not show up in the magnetic susceptibility. Similar phenomena have been observed in iron pnictides [10].

C. Model-fitting analysis

To further study the temperature dependence of the spectra, we performed model fitting for the optical conductivity data $\sigma_1(\omega)$. In order to compare with the previous work [18] on $CaFeO_3$, a similar model was applied to fit the data: $\sigma_1(\omega)$ was fit by the Drude-Lorentz model combined with the Fano functions for the phonons labeled by numbers 1 and 2 in Fig. 2(a). The Drude-Lorentz model has the following expression:

$$\sigma_1(\omega) = \frac{2\pi}{Z_0}\left[\frac{\Omega_p^2}{\omega^2\tau + \frac{1}{\tau}} + \sum_k \frac{\gamma_k \omega^2 \Omega_k^2}{\left(\omega^2 - \omega_{0,k}^2\right)^2 + \gamma_k^2 \omega^2}\right], \tag{2}$$

where Z_0 is the vacuum impedance. The first term describes the free-carrier Drude response, characterized by a plasma frequency Ω_p and a scattering rate $1/\tau$. The plasma frequency Ω_p satisfies $2\pi\Omega_p^2/Z_0 = ne^2/m$, with n being the carrier density. The second term describes a sum of Lorentz oscillators, each having a resonance frequency $\omega_{0,k}$, a line width γ_k, and an oscillator strength Ω_k. Fano functions have the form as follows [28–30]:

$$\sigma_1(\omega) = \frac{2\pi}{Z_0}\frac{\Omega_F^2}{\gamma_F}\frac{q^2 + 4q\epsilon - 1}{q^2(1 + 4\epsilon^2)}, \tag{3}$$

where $\epsilon = (\omega - \omega_F)/\gamma_F$, ω_F is the resonance frequency, γ_F represents the linewidth, and Ω_F corresponds to the strength. The asymmetry of the Fano line shape is described by a dimensionless parameter q. The phonons numbered 1 and 2 are fit by Fano functions, and other phonons are fit by Lorentz functions.

However, this model cannot fit the $\sigma_1(\omega)$ data around 1000 cm^{-1}, marked by the arrow in Fig. 2(a), because the broad mid-IR peak in the range 700–1500 cm^{-1} deviates from the Lorentz function. Scrutinizing the peak, one would find its asymmetric line shape: a fast increase from ~700 cm^{-1} to ~900 cm^{-1} followed by a slow decrease from ~900 cm^{-1} to ~1500 cm^{-1}. Such a structure has been observed in $La_{2-x}Sr_xCuO_4$ [15] and LSMO [5] and was explained as polaron excitation. A polaron is a quasiparticle formed by an electron dressed by a phonon cloud [31–33]. Historically, polarons were discovered and identified in doped semiconductors [31], while recently polaronic excitation has become an important issue in strongly correlated electronic systems. For example, in cuprates and manganites, the polaron effects and related strong electron-phonon interactions are necessary to understand the mechanisms of high-temperature superconductivity and colossal magnetoresistivity in these compounds [3,15].

In the present work, we fit the mid-IR peak in the $\sigma_1(\omega)$ data using the model of single-polaron absorption proposed by Gurevich *et al.* [20] with the following expression:

$$\sigma_1^p(\omega) = \eta\frac{\sqrt{\omega - \omega_0}}{\omega^3}, \tag{4}$$

where ω_0 is the threshold for polaronic absorption and the intensity prefactor $\eta = 2\alpha\omega_0^{3/2} n_p e^2/(3m)$, with α representing the electron-phonon coupling constant and n_p being the density of the polarons. This model can be deduced in the weak-coupling regime of the electron-phonon interaction. The formula has been applied to the polaronic absorption process in LSMO by Hartinger *et al.* [5]. In summary, we fit the $\sigma_1(\omega)$ data up to 15 000 cm^{-1} using one Drude term and three Lorentz terms for electronic excitation, one polaron term, two Fano terms for phonons labeled by numbers 1 and 2, as well as three additional Lorentz terms for other phonons. For illustration, the $\sigma_1(\omega)$ data at $T = 150$ K and its fitting curve are shown in Fig. 5.

Figure 6 shows the line shapes of phonons numbered 1 and 2, compared with the corresponding ones in the parent compound $CaFeO_3$. The number 1 and 2 phonons are related to the bending and stretching modes, respectively, which are closely connected to the CD transition in the parent compound [18]. Observed from Figs. 6(b) and 6(d), the asymmetry of

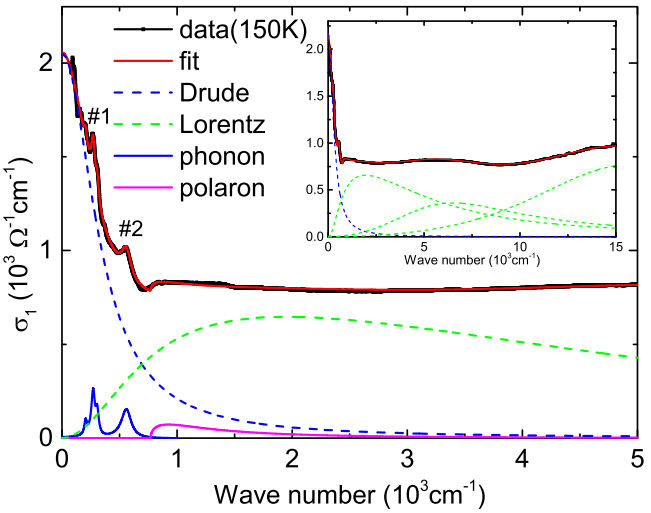

FIG. 5. Fitting curve of $\sigma_1(\omega)$ at $T = 150$ K. The inset shows the spectra up to 15 000 cm^{-1}.

phonon number 2 is less pronounced in $CaFe_{0.7}Co_{0.3}O_3$ than in $CaFeO_3$. Since phonon number 1 overlaps with other phonons around 260 and 300 cm^{-1}, shown in Fig. 6(a), its line shape cannot be clearly resolved. However, through fitting by the Fano functions in Eq. (3), we are able to extract the asymmetric factors $|1/q|$. Take $T = 15$ K for example, $|1/q| = 0.08$ for phonon number 1, and $|1/q| = 0.07$ for phonon number 2. They are much smaller than the ones found in $CaFeO_3$,

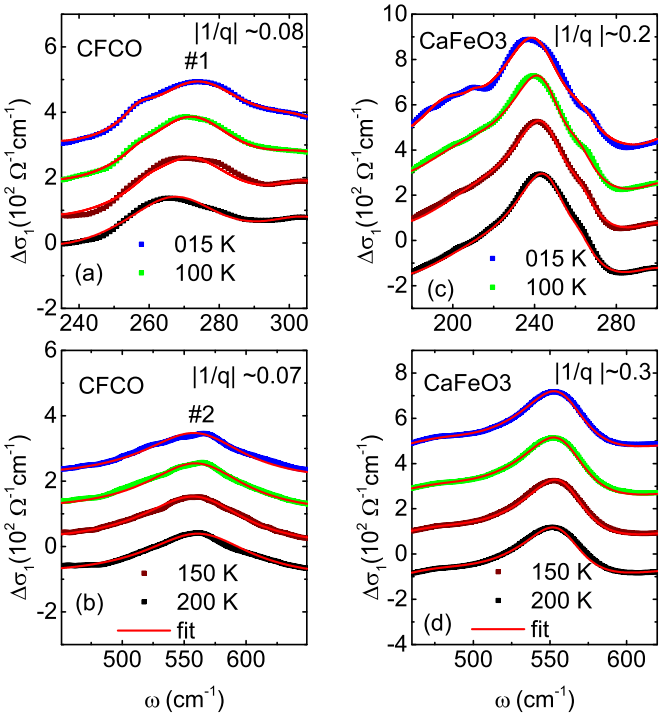

FIG. 6. (a), (b) Line shapes of phonons around 260 and 560 cm^{-1} in $CaFe_{0.7}Co_{0.3}O_3$. The Drude response and Lorentz term centered at ~2 000 cm^{-1} have been subtracted from the data. The curves are vertically shifted for clarity. (c), (d) The corresponding phonons in $CaFeO_3$. The red lines are fitting curves by the Fano profiles.

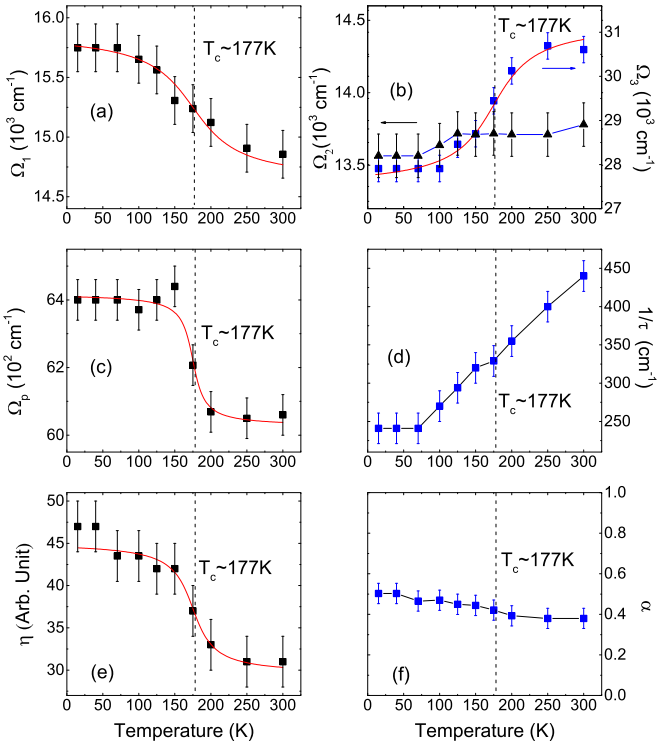

FIG. 7. (a), (b) Temperature dependence of the strength parameters Ω_1, Ω_2, and Ω_3 of the Lorentz oscillators centered at about 2000, 6000, and 15 000 cm^{-1}, respectively. (c) Temperature dependence of the plasma frequency Ω_p for the Drude component. (d) Temperature dependence of the scattering rate $1/\tau$ of the Drude component. (e) Polaron intensity η obtained from the fitting. (f) Temperature dependence of the electron-phonon coupling constant α.

which are ~0.2 and 0.3, respectively. The $|1/q|$ factors in $CaFe_{0.7}Co_{0.3}O_3$ do not change evidently with temperature, and $|1/q| < 0.1$ in the whole temperature range. The smaller $|1/q|$ factors imply [13,28] that the electron-phonon coupling in $CaFe_{0.7}Co_{0.3}O_3$ is weaker than in $CaFeO_3$.

Referring to the band structure [26] and the optical data [17] of $CaFeO_3$, we assign the Lorentz term centered at ~2000 cm^{-1} in Fig. 5 to interband excitation between Fe $3d$ e_g bands shown in Fig. 4(a), while the Lorentz terms centered at ~6000 cm^{-1} and ~15 000 cm^{-1} in the inset of Fig. 5 may be related to electronic excitations shown in Figs. 4(b) and 4(c) and/or excitations between occupied O $2p$ bands and Fe $3d$ e_g bands [17].

Figures 7(a) and 7(b) show the temperature dependence of the strength parameters Ω_1, Ω_2, and Ω_3 of the Lorentz components centered at about 2000, 6000 and 15 000 cm^{-1}, respectively. We find that Ω_1 increases and Ω_3 decreases with lowering temperature around $T_C \sim 177$ K, which is consistent with the discussion based on spectral weight analysis in Sec. III B. The temperature dependence of Ω_1 and Ω_3 can be fit by Eq. (1) with the parameters shown in Table I. From Fig. 7(b), we find that Ω_2 does not show evident change with temperature within error bars. These observations imply that Lorentz components centered about 2000 and 15 000 cm^{-1} correspond to type-1 and type-2 excitations shown in Fig. 4, respectively, while the Lorentz component centered at about

6000 cm^{-1} might be related to excitations between occupied O $2p$ bands and Fe $3d$ bands [17], which are not affected severely by the PM-FM transition.

Figures 7(c) and 7(d) summarize the fitting results of the Drude peak. The temperature dependence of the plasma frequency Ω_p is demonstrated in Fig. 7(c) and one notices an obvious increase of Ω_p with decreasing temperature around the FM transition, which is consistent with the spectral weight analysis shown in Fig. 3. Because Ω_p^2 is proportional to the charge carrier density, it implies that additional charge carriers are released or delocalized by the FM transition. Figure 7(d) shows the temperature dependence of the scattering rate of the Drude response, which is reduced upon cooling. As mentioned above, the broad peak around 1000 cm^{-1} is fit by the formula in Eq. (4) with two parameters, i.e., the intensity η and the threshold energy ω_0. We find that the parameter $\omega_0 = 750 \pm 10$ cm^{-1} is nearly unchanged with the varying temperature, while the parameter η increases with decreasing temperature, which accelerates around the Curie temperature T_C, as shown in Fig. 7(e). The temperature dependence of Ω_p and η is also fit by Eq. (1) with the parameters shown in Table I. We find that the Γ's are similar to the one for the magnetic susceptibility. It implies that the carriers or polarons are mainly released by the static ferromagnetic order, which is similar to the situation in doped manganites [35]. Compared with the temperature dependence of the spectral weight discussed in Sec. III B, the temperature evolution of Ω_p is sharper around T_C, which implies that the magnetic fluctuations do not affect Ω_p. Such fluctuated FM orders are dynamic and short ranged, which would have a characteristic time τ_F and a characteristic length l_F. If $\tau_F \ll \tau$ or $l_F \ll l$, where l is the mean free path, one would expect that the motion of the charge carriers related to the fluctuated short-range orders may not be coherent. Therefore, their optical response would not make an important contribution to the coherent Drude component.

The observation that both the plasma frequency Ω_p and the polaron intensity η increase evidently around the Curie temperature implies that the densities of the carrier and the polaron are enhanced by the PM-FM transition. Such two simultaneous phenomena can be understood together, if one considers the Drude peak and the polaron peak as two kinds of excitations of the polarons [4]. The Drude peak corresponds to the coherent excitation of the carriers with the deformed lattice, i.e., the collective motion of charges dressed by the phonon clouds (large polarons). On the other hand, the mid-IR peak with a relatively higher energy is related to stripping the charge out of the phonon cloud. Both of the excitations are enhanced by the FM transition in the presence of Hund's interaction, just as the FM transition increases the polaronic excitation in LSMO [4,34]. As both the Drude peak and the polaronic peak are optical responses of the polarons, it might be reasonable to assume that the carrier density n in the Ω_p^2 of the Drude term of Eq. (2) is equal to the polaron density n_p, i.e., $n = n_p$. Taking advantage of this assumption, we can replace the quantity $n_p e^2/m$ in the prefactor η of Eq. (4) by $2\pi\Omega_p^2/Z_0$, and estimate the electron-lattice coupling constant α. From Fig. 7(f), we can see that $\alpha \sim 0.4$–0.5, which does not show obvious temperature dependence within error bars. Such an electron-phonon coupling falls into the weak-coupling regime [31], which is consistent with the assumption of the fitting model in Eq. (4). Based on the model of Millis *et al.* [3], in the weak-coupling regime of the electron-phonon interaction, the magnetic transition transforms a PM metallic state to an FM metallic state upon cooling. Interestingly, we notice that $CaFe_{0.7}Co_{0.3}O_3$ shows the same transition from a PM metal to an FM metal, which is exactly what we expect for the weak-coupling regime of the model of Millis *et al.* [3].

IV. SUMMARY AND CONCLUSIONS

We studied the optical properties of $CaFe_{0.7}Co_{0.3}O_3$. In sharp contrast to the parent compound $CaFeO_3$, $CaFe_{0.7}Co_{0.3}O_3$ does not undergo a CD transition and is a metal in the whole temperature range. The experimental results of the reflectivity and optical conductivity of $CaFe_{0.7}Co_{0.3}O_3$ have been presented. As the temperature is lowered, the Drude peak intensifies and the scattering rate decreases; meanwhile the spectral weight is transferred from 4800–14 000 cm^{-1} to 0–4800 cm^{-1}. The spectral weight transfer accelerates around the Curie temperature $T_C \sim 177$ K, which indicates that the PM-FM transition is the driving force of the transfer. Similar to the explanation for doped manganites [24,35], we explained the spectral weight transfer in the scenario of Hund's coupling. In the FM phase, the spins polarize and the energy of electronic excitations decreases according to the Hund's rule, which leads to the spectral weight transfer from high to low energy.

In doped perovskites, electron-phonon interaction often manifests itself as polaronic peaks in optical spectra [14,33]. In the present work, the broad peak in the mid-IR region of the optical conductivity is explained as polaronic excitation and is fit by the model of Gurevich *et al.* [20]. We find that the threshold energy ω_0 which is related to the polaronic binding energy is temperature independent, and that the intensity η increases with decreasing temperature, especially around T_C. From the fitting parameters of the polaron peak, we are able to estimate the electron-lattice coupling constant $\alpha \sim 0.4$–0.5, which is much smaller than $\alpha \sim 5$ in LCMO [4] and is also smaller than the one found in LSMO with $\alpha \sim 1$ [5]. This is in good agreement with the theory of Millis *et al.* [3]: LCMO falls into the intermediate-coupling regime and transforms from an insulating PM to metallic FM state upon cooling, while CFCO falls into the weak-coupling regime and undergoes a metallic PM-FM transition.

Comparing the phonon line shapes of $CaFe_{0.7}Co_{0.3}O_3$ with the ones of $CaFeO_3$, we find that $CaFe_{0.7}Co_{0.3}O_3$ shows minor asymmetric line shapes, which is in sharp contrast to the case in the parent compound [18]. It might imply that the substitution of Fe with Co would reduce the electron-phonon interaction in this system, and that the electron-lattice interaction plays important roles in the CD transition of the parent compound.

ACKNOWLEDGMENTS

We thank L. Yu for helpful discussion. This work was supported by the MOST of China (973 Projects No. 2015CB921303, No. 2015CB921102, No.2014CB921500) and NSFC (Grants No. 91421304, No. 11374345, No. 11574378).

[1] M. Imada, A. Fujimori, and Y. Tokura, Rev. Mod. Phys. **70**, 1039 (1998).

[2] M. B. Salamon and M. Jaime, Rev. Mod. Phys. **73**, 583 (2001).

[3] A. J. Millis, Boris I. Shraiman, and R. Mueller, Phys. Rev. Lett. **77**, 175 (1996).

[4] K. H. Kim, J. H. Jung, and T. W. Noh, Phys. Rev. Lett. **81**, 1517 (1998).

[5] Ch. Hartinger, F. Mayr, J. Deisenhofer, A. Loidl, and T. Kopp, Phys. Rev. B **69**, 100403(R) (2004).

[6] Ch. Hartinger, F. Mayr, A. Loidl, and T. Kopp, Phys. Rev. B **73**, 024408 (2006).

[7] P. M. Woodward, D. E. Cox, E. Moshopoulou, A. W. Sleight, and S. Morimoto, Phys. Rev. B **62**, 844 (2000).

[8] S. Kawasaki, M. Takano, R. Kanno, T. Takeda, and A. Fujimori, J. Phys. Soc. Jpn. **67**, 1529 (1998).

[9] N. L. Wang, W Z Hu, Z. G. Chen, R. H. Yuan, G. Li, G. F. Chen, and T. Xiang, J. Phys.: Condens. Matter **24**, 294202 (2012).

[10] B. Xu, Y. M. Dai, H. Xiao, B. Shen, Z. R. Ye, A. Forget, D. Colson, D. L. Feng, H. H. Wen, X. G. Qiu, and R. P. S. M. Lobo, Phys. Rev. B **94**, 085147 (2016).

[11] Y. Takahashi, N. Kida, Y. Yamasaki, J. Fujioka, T. Arima, R. Shimano, S. Miyahara, M. Mochizuki, N. Furukawa, and Y. Tokura, Phys. Rev. Lett. **101**, 187201 (2008).

[12] B. Xu, Y. M. Dai, B. Shen, H. Xiao, Z. R. Ye, A. Forget, D. Colson, D. L. Feng, H. H. Wen, C. C. Homes, X. G. Qiu, and R. P. S. M. Lobo, Phys. Rev. B **91**, 104510 (2015).

[13] B. Xu *et al.*, Nat. Commun. **8**, 14933 (2017).

[14] R. P. S. M. Lobo, F. Gervais, and S. B. Oseroff, Europhys. Lett. **37**, 341 (1997).

[15] A. Lucarelli, M. Ortolani, A. Perla, S. Lupi, P. Maselli, and P. Calvani, Int. J. Mod. Phys. B **17**, 521 (2003).

[16] Ch. Hartinger, F. Mayr, A. Loidl, and T. Kopp, Phys. Rev. B **70**, 134415 (2004).

[17] J. Fujioka, S. Ishiwata, Y. Kaneko, Y. Taguchi, and Y. Tokura, Phys. Rev. B **85**, 155141 (2012).

[18] C. X. Zhang, H. L. Xia, H. Liu, Y. M. Dai, B. Xu, R. Yang, Z. Y. Qiu, Q. T. Sui, Y. W. Long, S. Meng, and X. G. Qiu, Phys. Rev. B **95**, 064104 (2017).

[19] H. L. Xia. Y. Y. Yin, J. H. Dai, J. Y. Yang, X. M. Qin, C. Q. Jin, and Y. W. Long, Mater. Res. Express **2**, 046103 (2015).

[20] V. Gurevich, I. Lang, and Y. Firsov, Sov. Phys. Solid State **4**, 918 (1962).

[21] Y. Long, Y. Kaneko, S. Ishiwata, Y. Taguchi, and Y. Tokura, J. Phys.: Condens. Matter **23**, 245601 (2011).

[22] Y. W. Long, Y. Kaneko, S. Ishiwata, Y. Tokunaga, T. Matsuda, H. Wadati, Y. Tanaka, S. Shin, Y. Tokura, and Y. Taguchi, Phys. Rev. B **86**, 064436 (2012).

[23] C. C. Homes, M. Reedyk, D. A. Cradles, and T. Timusk, Appl. Opt. **32**, 2976 (1993).

[24] A. Nucara, P. Calvani, F. Crispoldi, D. Sali, S. Lupi, C. Martin, and A. Maignan, Phys. Rev. B **73**, 054425 (2006).

[25] S. Ghosh, N. Kamaraju, M. Seto, A. Fujimori, Y. Takeda, S. Ishiwata, S. Kawasaki, M. Azuma, M. Takano, and A. K. Sood, Phys. Rev. B **71**, 245110 (2005).

[26] T. Saha-Dasgupta, Z. S. Popovic, and S. Satpathy, Phys. Rev. B **72**, 045143 (2005).

[27] C. Lacroix-Lyon-Caen and M. Cyrot, Solid State Comm. **21**, 837 (1977).

[28] W. J. Padilla, M. Dumm, S. Komiya, Y. Ando, and D. N. Basov, Phys. Rev. B **72**, 205101 (2005).

[29] A. B. Kuzmenko, L. Benfatto, E. Cappelluti, I. Crassee, D. van der Marel, P. Blake, K. S. Novoselov, and A. K. Geim, Phys. Rev. Lett. **103**, 116804 (2009).

[30] B. Xu, Y. Dai, J. Han, K. Wang, R. Yang, Y. Yang, W. Zhang, H. Xiao, and X. Qiu, Physica C: Superconductivity **503**, 25 (2014).

[31] P. Calvani, Riv. Nuovo Cimento **24**, 1 (2001).

[32] J. T. Devreese, S. N. Klimin, J. L. M. van Mechelen, and D. van der Marel, Phys. Rev. B **81**, 125119 (2010).

[33] E. Cappelluti, S. Ciuchi, and S. Fratini, Phys. Rev. B **79**, 012502 (2009).

[34] A. Machida, Y. Moritomo, and A. Nakamura, Phys. Rev. B **58**, R4281(R) (1998).

[35] Y. Okimoto, T. Katsufuji, T. Ishikawa, A. Urushibara, T. Arima, and Y. Tokura, Phys. Rev. Lett. **75**, 109 (1995).